Worst Case Timing Jitter and Amplitude Noise in Differential Signaling

Wei Yao, Yiyu Shi, Lei He, Sudhakar Pamarti and Yu Hu
Electrical Engineering Dept., University of California, Los Angeles, CA, 90095, USA
{weiyao, yshi, lhe, spamarti, hu}@ee.ucla.edu

Abstract— Differential signaling is widely used in high speed data communications. Inter-symbol interference (ISI) and crosstalk between differential pair, however, heavily affect the integrity of differential signaling as measured by timing jitter and amplitude noise in the eye diagram. To reduce the impact of ISI, a pre-emphasis filter is commonly used, but it increases the crosstalk noise. In this paper, we first propose formula-based jitter and noise models considering the combined effect of ISI, crosstalk, and pre-emphasis filter. With given input patterns, our models achieve within 5% difference compared to SPICE simulation. Moreover, using the formula-based models, we develop mathematical programming algorithms to directly find out the input patterns for worst-case jitter and worst-case amplitude noise. Experiments show our algorithms obtain more reliable worst-case jitter and noise compared to Monte Carlo simulation and reduce runtime by 150×.

Keywords—Transmission line, Jitter, Amplitude noise, Modeling.

I. Introduction

Differential signaling has been widely used in high-speed I/O interconnect standards like PCI-Express and Serial ATA. It has several advantages, such as a high transmission rate due to low signal swing, little electromagnetic interference (EMI), and common-mode noise immunity. Considerable signal integrity issues, however, still limit the link performance and become bottlenecks during system integration. Such issues include resistive losses, reflections, inductive ringing and crosstalk between differential pairs [1, 2].

To evaluate the combined effect of these impairments on the overall system performance, the associated eye diagram [3, 4] has been used as an effective measure. As shown in Fig. 1, the eye diagram is defined as the synchronized superposition of all possible realizations of the signal viewed within a particular signal interval. It provides a fast evaluation of system performance. The width of the eye opening defines the time interval over which the received signal can be sampled without error. The height of the eye opening with the amount of amplitude noise at a specified sampling time defines the signal-to-noise-ratio of the received signal [3].

Consider the eye diagram shown in Fig. 1. The amounts of timing jitter and amplitude noise determine the width and height of the eye. Jitter is defined as the deviation

This paper is partially supported by a UC MICRO grant sponsored by Actel and Fujitsu. Address comments to lhe@ee.ucla.edu.

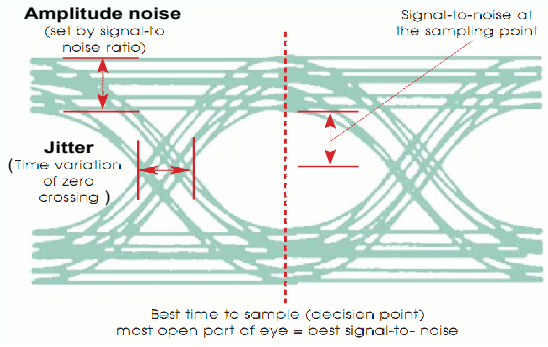

Fig. 1. Eye diagram

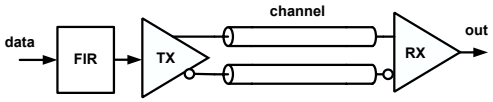

Fig. 2. Transceiver for differential signaling

of the zero-crossing from its ideal occurrence time and decreases the eye's width [5]. Amplitude noise, on the other hand, decreases the signal-to-noise ratio (SNR) and, accordingly, the eye's height. As a result, to determine the performance of the interconnect, we need to consider both timing jitter and amplitude noise simultaneously.

Specifically, inter-symbol interference (ISI) and crosstalk are two major factors that induce jitter and amplitude noise. ISI is defined as one symbol interfering with subsequent symbols and is caused by channel impairments such as attenuation, reflection, and group delay distortion. Crosstalk, on the other hand, is caused by electromagnetic coupling between transmission lines. To counteract ISI, a finite impulse response (FIR) pre-emphasis filter at the transmitter side is widely used to emphasize the signal prior to the impact of the channel [6–8]. However, pre-emphasized signal couples more electromagnetic energy into neighboring channels and may exacerbate the crosstalk.

Traditionally, the eye diagram is obtained through lengthy simulations or measurements. In literature, several types of techniques are proposed to model the eye diagram and try to efficiently predict the jitter and amplitude noise at the design phase [9–12]. However, [9] considers reflection and attenuation with only one input pattern, and [10] only considers a lossless transmission line. As a result, those models are far from accurate. [12] and [11] have a better model because they consider lossy transmission lines, but they still take only a few input patterns into account and

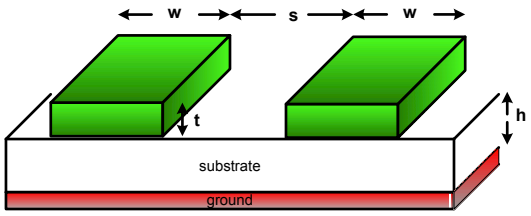

Fig. 3. Section of differential microstrip line

use an inaccurate linear approximation. The efficient handling of input patterns in adequate length is still an open question. Most importantly, all existing works fail to consider the effect of the pre-emphasis filter, which effectively reduces ISI, as shown in Fig. 6 in Section II, but may increase crosstalk.

In this paper, we first propose formula-based jitter and amplitude noise models that consider the combined effect of ISI, crosstalk, and the pre-emphasis filter. We apply a RLGC lossy transmission line model according to differential microstrip line geometry, and we represent the channel impairments and crosstalk through transmission line time domain response. With given input patterns, our models achieve within 5% difference compared to SPICE simulation. Using the formula-based models, we then develop mathematical programming algorithms to directly predict the input patterns that cause worst-case jitter and worst-case amplitude noise. Experiments show our algorithms obtain more reliable worst-case jitter and noise compared to Monte Carlo simulation and reduce runtime by 150×.

The rest of this paper is organized as follows: Section II reviews background on transmission lines and the pre-emphasis filter. Section III presents our formula-based jitter and noise models. Section IV introduces our mathematical programming algorithms, and section V describes experiments on different transmission lines. Section VI concludes the paper.

II. Backgrounds

A. RLGC Model

A cross-section of the differential microstrip line is shown in Fig. 3. We assume the lines are homogeneous, uniform, and parallel to each other without any variation [10]. The dielectric is assumed to be homogeneous with constant permittivity ε and permeability μ.

The distributed self and mutual inductances are computed with the method of images [13]: the effect of the ground plane is replaced with the image currents. Using the notations from Fig. 3, the following expressions were found for the per-unit-length self and mutual inductances [13]:

$$l = \frac{\mu}{2\pi} ln\left(1 + \frac{2H_{eq}}{r_{eq}}\right) \tag{1}$$

$$m = \frac{\mu}{4\pi} ln\left(\frac{(s_{eq}+2r_{eq})^2 + (r_{eq}+2H_{eq})^2}{(s_{eq}+2r_{eq})^2 + r_{eq}^2}\right). \tag{2}$$

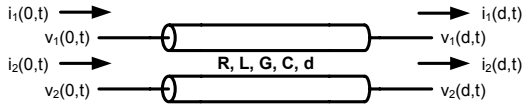

Fig. 4. Parallel transmission lines

The distributed capacities may be calculated as follows [14]

$$c_p = \frac{\mu\epsilon m}{l^2 + m^2} \tag{3}$$

$$c = \frac{\mu\epsilon l}{l^2 + m^2}. \tag{4}$$

B. Parallel Transmission Lines

High-speed signal propagation on an interconnect can be influenced by several effects, such as delay, attenuation, reflection, slew rate limitation, and crosstalk. All of these effects, which are also known as transmission line effects [15], can be captured by Telegrapher's equations using RLGC per-unit-length model [15].

Consider the transmission line pair shown in Fig. 4. In frequency domain, the voltage-current relationships between $x = 0$ and $x = d$ [15] can be expressed as

$$\begin{aligned}\begin{bmatrix} I(0) \\ -I(d) \end{bmatrix} &= \begin{bmatrix} Y_{11} & Y_{12} \\ Y_{21} & Y_{22} \end{bmatrix} \begin{bmatrix} V(0) \\ V(d) \end{bmatrix} \\ &= \begin{bmatrix} W_i E_1 W^{-1} & W_i E_2 W^{-1} \\ W_i E_2 W^{-1} & W_i E_1 W^{-1} \end{bmatrix} \begin{bmatrix} V(0) \\ V(d) \end{bmatrix}\end{aligned} \tag{5}$$

where

$$E_1 = diag\{\frac{1 + e^{-2\gamma_k d}}{1 - e^{-2\gamma_k d}}\} \tag{6}$$

$$E_2 = diag\{\frac{-2e^{-2\gamma_k d}}{1 - e^{-2\gamma_k d}}\}, \qquad k = 1, 2, \ldots, N \tag{7}$$

$$W^{-1}ZYW = \begin{bmatrix} \gamma_1^2 & 0 & 0 \\ 0 & \cdots & 0 \\ 0 & 0 & \gamma_N^2 \end{bmatrix} = \Gamma^2, \tag{8}$$

with $W_i = Z^{-1}W\Gamma$, $I(0)$, $I(d)$, $V(0)$ and $V(d)$ are Laplace transforms of $i(0,t)$, $i(d,t)$, $v(0,t)$ and $v(d,t)$, respectively. $Z = R + sL$ and $Y = G + sC$ are the impedance and admittance matrices. The transformation matrix W corresponds to the eigenvectors of product ZY and the resulting diagonal matrix contains the corresponding eigenvalues.

C. Pre-emphasis Filter

Using a symbol-spaced finite impulse response (FIR) filter to pre-emphasize the signal at the transmitter end is a common way to counteract ISI. The filter can be expressed as

$$y(n) = \sum_{i=-N}^{M} W_i x(n-i). \tag{9}$$

A circuit implementation of the current-mode logic (CML) pre-emphasis driver is shown in Fig. 5. The coefficient of each tap is realized by the current source and requires a dedicated differential pair to drive the output.

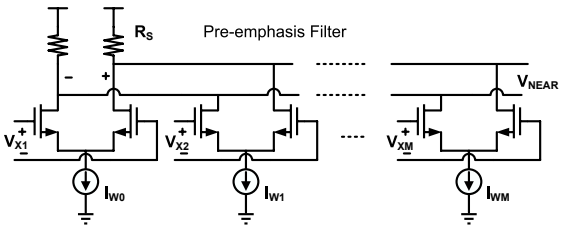

Fig. 5. Pre-emphasis filter at transmitter end for CML differential signaling

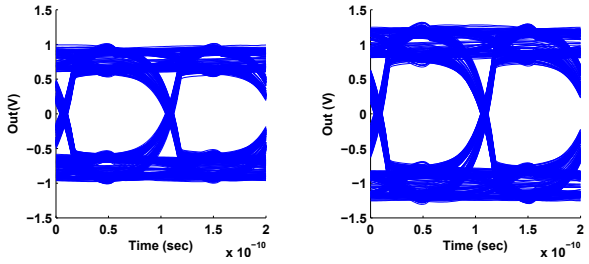

Fig. 6. Eye diagram (left) without the pre-emphasis filter and (right) with applying a 4-taps pre-emphasis filter

Normally, the number of taps ranges from 2 to 5 because of power and area constraints.

The coefficient of each tap is directly related to the channel characteristic mentioned in the previous sub-section and can be determined adaptively by the least-mean-square (LMS) algorithm [6, 7]:

$$W_i^{k+1} = W_i^k + \mu \epsilon_k x_{k-i}, \tag{10}$$

where W is the tap coefficient and μ is the step size. ϵ_k is the error signal and is defined as the difference between the received signal value and the transmitted value. The convergence of errors drives the coefficients to their optimal value.

To demonstrate the effectiveness of the pre-emphasis filter, the eye diagram with and without the pre-emphasis filter is compared in Fig. 6. The SNR improvement can be clearly seen. As a result, jitter and amplitude noise models can't capture the actual link performance without considering the existence of pre-emphasis filter.

III. Jitter and Amplitude Noise Model

The jitter and amplitude noise are actual stochastic processes and can be divided into two categories: random and deterministic. The random part is usually described through a probability density function(pdf) or its root-mean-square(rms) value. On the other hand, the deterministic part is predictable and makes the dominant contribution to the shape of eye diagram [16]. To start with, we model the CML transmitter as an independent voltage source, V_s, with matching conductance G_s. At the receiver end, G_L and C_L are used to model the loading conductance and parasitic capacitance of the CML receiver, as shown in Fig. 7. Therefore, the termination constraints become

$$V(0) = V_s - \frac{I(0)}{G_s} \tag{11}$$

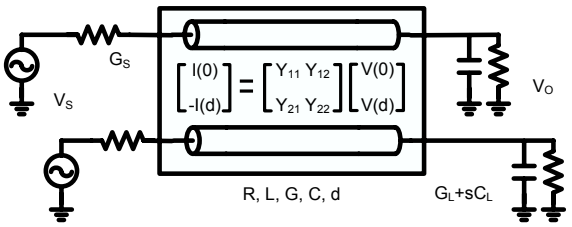

Fig. 7. Differential signaling with parallel transmission lines and termination

and

$$I(d) = (G_L + sC_L)V(d), \tag{12}$$

and we can derive the frequency domain transfer function using (5), (11) and (12). The result is as follows:

$$V(d) = \tilde{H}V_s(s) = (Y_{12} + (Gs + Y_{11})\tilde{Y})^{-1}Gs \cdot V_s(s), \tag{13}$$

where

$$\tilde{Y} = Y_{21}^{-1}(-Y_{22} - G_L - sC_L). \tag{14}$$

Note that G_s, G_L, and C_L are all 2×2 diagonal matrices. $\tilde{H}$ describes the complete two-port relationship and includes the effect of ISI, crosstalk, reflection, and all other channel impairments. The frequency domain relationship between differential input and differential output now becomes

$$H(s) = \begin{bmatrix} 1 & -1 \end{bmatrix} \tilde{H} \begin{bmatrix} \frac{1}{2} \\ -\frac{1}{2} \end{bmatrix}. \tag{15}$$

In order to find the time domain response, (15) is approximated into the following pole-residue form:

$$H(s) = c + \sum_{i=1}^{q} \frac{k_i}{s - p_i}, \tag{16}$$

by using a least-square-approximation-based method [17]. In this way, the time domain step response can be obtained through the inverse Laplace transform of $H(s)/s$ and we get

$$s(t) = c \cdot u(t) + \sum_{i=1}^{q} \frac{k_i}{p_i}(e^{p_i t} - 1)u(t). \tag{17}$$

The received signal at the far-end of the transmission line now can be expressed as

$$r(t) = \sum_{i=-\infty}^{\infty} b_i p(t - iT), \tag{18}$$

where

$$p(t) = s(t) - s(t - T), \tag{19}$$

is the time-domain response of a non-return-to-zero (NRZ) symbol, and b_i can be evaluated as

$$b_i = \sum_{j=0}^{m-1} W_j a_{i+j}, \tag{20}$$

with W_j as the pre-emphasis filter coefficient and a_i as the input symbol pattern. m is the number of taps in the filter.

We define the reference time point t_0 as the time when the waveform, without interference from neighboring symbols, crosses a certain threshold V_{th} [11]. In other words, t_0 can be solved with

$$p(t_0) = V_{th}, \quad 0 \le t_0 < T. \tag{21}$$

Jitter is the deviation from such a time point. For a given input pattern, the jitter can be computed as

$$|t_1 - t_0|, \tag{22}$$

where

$$r(t_1) = V_{th}. \tag{23}$$

On the other hand, the amplitude noise is defined as the amplitude variation at the optimal sampling time, that is

$$|r(t_s) - p(t_s)|, \tag{24}$$

where

$$t_s = \arg\max_t \{p(t)\}. \tag{25}$$

Note that $r(t)$ attenuates quickly as time goes toward infinity. Thus (23) can be well approximated by

$$\sum_{i=-N}^{N} b_i r(t_1 - iT) = V_{th}, \tag{26}$$

where N can be decided such that the error is within a certain bound

$$|b_N r(t - NT)| < |\epsilon r(t)|, \forall 0 \le t < T, \tag{27}$$

and ϵ is in $[0, 1]$ and is specified by the user. A larger ϵ reduces the problem complexity, but introduces more significant error.

IV. Worst-case Jitter and Amplitude Noise

The deterministic part of jitter and amplitude noise highly depends on the input pattern. As a result, it is critical to find out the worst-case input pattern without doing lengthy simulations, as will be discussed in this section.

A. Worst-case Timing Jitter

The worst jitter is the sum of the worst positive deviation $t_1 - t_0$ ($t_1 > t_0$) and the worst negative deviation $t_0 - t_1$ ($t_0 > t_1$). For simplicity of presentation, we only discuss how to compute the worst positive deviation. It should be understood that the same procedure can be applied to compute the worst negative deviation as well. We can formulate the worst positive deviation as the following integer non-convex programming problem (**P1**)

$$\begin{aligned}
(\mathbf{P1}) \quad \max_{a_i} \quad & t_1 - t_0 && (28)\\
s.t. \quad & \sum_{i=-\infty}^{\infty} b_i r(t_1 - iT) = V_{th} && (29)\\
& t_0 \le t_1 < T && (30)\\
& b_i = \sum_{j=0}^{m-1} W_j a_{i+j} && (31)\\
& a_i \in \{0, 1\}, && (32)
\end{aligned}$$

B. Relaxation Based Binary Search

If we assign a set of values to t_1, then the problem becomes a non-linear feasibility problem and can be solved through an efficient heuristic method, i.e., for each value of t_1, we test whether a combination of the symbols a_i can be found such that (29) holds, and then pick the t_1 that maximizes $t_1 - t_0$ among all the feasible solutions. Such a problem structure enables us to use the binary search technique on t_1, which is bounded in $[t_0, T)$. However, the main difficulty lies in the fact that the feasible space for t_1 is not continuous. If we randomly assign values to t_1, the chance for it to be feasible is slim.

To overcome this difficulty, instead of finding a set of symbols that satisfies (29), we look for a nearby feasible value as an alternative, if possible. This is done by the following procedure. Suppose t_1 is assigned with value $\tilde{t}_1$. Then the corresponding feasibility problem would be

$$\begin{aligned}
& \sum_{j=-N}^{N} b_j r(\tilde{t}_1 - jT) = V_{th} && (33)\\
& 0 \le \tilde{t}_1 < T && (34)\\
& b_j = \sum_{i=0}^{m-1} W_i a_{i+j} \quad -N \le j \le N && (35)\\
& a_j \in \{0, 1\} \quad -N \le j \le N + m - 1, && (36)
\end{aligned}$$

Instead of solving it directly, we relax the integer constraint (36) to

$$0 \le a_j \le 1 \quad -N \le j \le N + m - 1, \tag{37}$$

and solve the problem (**P2**)

$$\begin{aligned}
(\mathbf{P2}) \quad \max \quad & \sum_{j=-N}^{N+m-1} |a_j - 0.5| && (38)\\
s.t. \quad & b_j = \sum_{i=0}^{m-1} W_i a_{i+j} \quad -N \le j \le N && (39)\\
& \sum_{j=-N}^{N} b_j r(\tilde{t}_1 - jT) = V_{th} && (40)\\
& 0 \le a_j \le 1 \quad -N \le j \le N + m - 1 && (41)
\end{aligned}$$

The objective function (38) tries to find the solution set a_j that is as close to the integer as possible. For the time being, let's assume that we know how to solve (**P2**). Then we denote the optimal solution as $\tilde{a}_j$ and round it to 0 or 1. After that, we can get $\tilde{b}_j$ from (39), and insert them in the equation

$$\sum_{j=-N}^{N} \tilde{b}_j r(t_1 - jT) = V_{th} \tag{42}$$

to solve for t_1, which is close to $\tilde{t}_1$ and yet is a feasible solution of the original problem. This procedure can now be used as the core for the binary search. The overall

algorithm for jitter computation is shown in Algorithm 1, where ϵ_0 is used to control the termination condition: when the lower bound and upper bound have a difference smaller than ϵ_0, the search stops.

Now we discuss how problem (**P2**) can be solved efficiently. For the sake of efficiency, we propose an heuristic to obtain its solution directly from the structure of (**P2**). Let

$$x_j = a_j - 0.5 \quad -N \le j \le N+m-1, \tag{43}$$

and insert (39) into (40). Then(**P2**) can be transformed into an equivalent form

$$\max \quad \sum_{j=-N}^{N+m-1} |x_j| \tag{44}$$

$$s.t. \quad \sum_{j=-N}^{N+m-1} c_j x_j = d \tag{45}$$

$$-0.5 \le x_j \le 0.5 \quad -N \le j \le N+m-1, \tag{46}$$

where c_j and d are some constants that can be derived easily.

The incentive of the heuristic to be proposed below is to let as many x_i take the maximum absolute value as possible. Due to the symmetry of the problem, without loss of generosity, we can assume

$$|c_{-N}| \le |c_{-N+1}| ... \le |c_k| \le |c_{k+1}| \le |c_{N+m-1}| \tag{47}$$

Then according to this ascending order of $|c_i|$, we assign -0.5 or 0.5 as the optimal value $\tilde{x}_i$ based on the following criteria

$$\tilde{x}_i = \begin{cases} -sgn(c_i) \times 0.5 & \text{if } d - \sum_{j=-N}^{i-1} c_j x_j > 0 \\ sgn(c_i) \times 0.5 & otherwise \end{cases} \tag{48}$$

This assignment is continued until

$$\sum_{j=i+1}^{N+m-1} 0.5|c_j| < d - \sum_{j=-N}^{i} c_j \tilde{x}_j. \tag{49}$$

And the solutions for the remaining x_i are

$$\tilde{x}_i = sgn(c_i) \times \frac{\sum_{j=-N}^{i} c_j \tilde{x}_j - d}{|c_i|}. \tag{50}$$

Note that due to the complexity of the original problem, we cannot guarantee that the solution obtained from our algorithm is optimal (or even locally-optimal). However, experimental results show that our algorithm gives a result that is very close or more pessimistic to the enumeration method, yet achieves significant speedup.

C. Worst-case Amplitude Noise

The amplitude noise is the difference between the maximum amplitude deviation and the minimum amplitude deviation, at the optimal sampling time. To find the worst-case noise, we could use the following formulation:

Algorithm 1 Algorithm for solving problem (**P1**).

Initialize: $t_1^{lb} = t_0$; $t_1^{ub} = T$;
while $t_1^{lb} < t_1^{ub} - \epsilon_0$ **do**
  $\tilde{t}_1 = (t_1^{lb} + t_1^{ub})/2$;
  Solve problem (**P2**) for $\tilde{a}_i$ and round it to 0 or 1.
  Compute $\tilde{b}_i$ based on the rounded $\tilde{a}_i$ from (39);
  Solve (42) for t_1;
  if $t_1 > t_1^{lb}$ **then**
    $t_1^{lb} = t_1$;
  else
    $t_1^{ub} = \tilde{t}_1$;
  end if
end while
Return t_1^{lb};

$$(\mathbf{P3}) \quad \max_{a_i} \text{ or } \min_{a_i} \quad \sum_{i=-N}^{N} b_i r(t_s - iT) \tag{51}$$

$$s.t. \quad b_i = \sum_{j=0}^{m-1} W_j a_{i+j} \tag{52}$$

$$a_i \in \{0,1\}, \tag{53}$$

where

$$t_s = \arg\max_t \{p(t)\} \tag{54}$$

is the optimal sampling time. The difference between maximum and minimum deviation determines the peak-to-peak amplitude noise for the eye diagram. Given the t_s calculated from (54), we can rewrite (**P3**) as (use the maximum problem as an example)

$$\max_{a_i} \quad \sum_{i=-N}^{N+m-1} c_i a_i \tag{55}$$

$$s.t. \quad a_i \in \{0,1\} \tag{56}$$

where c_i again is some constant that can be derived easily. As a result, it is a linear programming problem and, moreover, the solution can be obtained directly without calling the general linear programming solver. Obviously, to maximize the objective function, we just let a_i be 1 if c_i is positive and be 0 if c_i is negative [18]. For the minimum case, it is vice versa. So the amplitude noise can be expressed as

$$\sum_{i=-N}^{N+m-1} |c_i|. \tag{57}$$

V. Experimental Results

In this section, we report our experiments on a Pentium 4 computer with 2.66G CPU and 1G RAM.

A. Jitter and Amplitude Noise Model Validation

To start with, we first verify our transmission line channel model. Table I lists the detailed design information for our various testbench. And Fig. 8 shows the comparison of the transient simulation result between our analytical channel model and SPICE simulation for Design 1. From Fig. 8, we

TABLE I

DIFFERENTIAL TRANSMISSION LINE TESTBENCH DESIGN INFORMATION: WIDTH(W), SPACING(S), THICKNESS(T), DIELECTRIC HEIGHT(H), LENGTH(L) AND CHARACTERISTIC IMPEDANCE.

Design	w (um)	s (um)	t (um)	h (um)	L (cm)	Char. impedance
#1	100	193.86	10	300	15	49.03
#2	50	117.48	50	200	15	49.2
#3	50	117.48	50	200	25	49.2
#4	100	80	10	300	15	52.51
#5	50	500	10	300	30	58.55

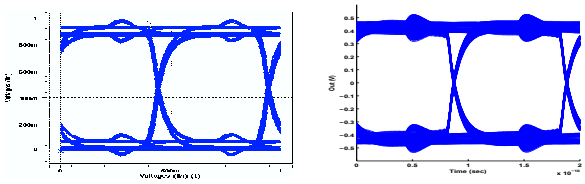

Fig. 8. Transient simulation comparison between (left) SPICE and (right) our model. The origin point is different.

TABLE II

JITTER AND AMPLITUDE NOISE MODEL VALIDATION, GIVEN THE SAME INPUT PATTERN.

	SPICE			Our Model		
	Jitter (ps)	Noise (V)	Runtime (sec)	Jitter (ps)	Noise (V)	Runtime (sec)
#1	11.8	0.27	0.26	11.9	0.27	0.17
#2	5.0	0.20	0.26	5.0	0.21	0.17
#3	4.6	0.20	0.25	4.7	0.19	0.16
#4	11.0	0.29	0.26	10.5	0.30	0.17
#5	7.7	0.11	0.23	7.7	0.11	0.18

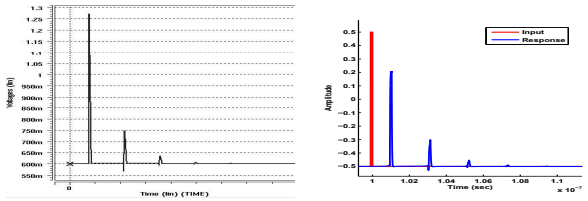

Fig. 9. Time domain response: SPICE simulation(left) and MATLAB simulation with our model(right). The origin point is different.

can find out that the transient behavior is pretty similar and both give the same amount of timing jitter and amplitude noise. Note that the origin point is different between SPICE and our model. This is due to different input setting and does not affect the noise and jitter measurement.

Next, we verify our jitter and noise model with SPICE given the same set of input patterns in Table II. The test pattern contains 100 symbol with a data rate at 10Gb/s. From Table II, we discover that, given the same input pattern, our model can accurately calculate jitter and noise with similar runtime, compared to SPICE results. The error is within 4.5% for jitter and 5% for noise. Although the runtime improvement is not much, our model is easier to be embedded into other tools or algorithms.

To emphasize the importance of considering a long period of time domain response, Fig. 9 shows the time domain response for Design 5, but with unmatched termination resistance. The impedance mismatch at the receiver end will cause severe signal reflection. From Fig. 9, both SPICE simulation and our model clearly illustrate the signal reflection behavior. As a result, only a few taps of time domain response is not sufficient to determine the jitter and noise performance.

B. Worst-case Jitter and Amplitude Noise Calculation

The worst-case jitter, amplitude noise, and runtime comparison for various design cases are listed in Table III. The pre-emphasis filter is optimized in advance for different channel characteristics. The jitter and amplitude performance is calculated through our formula-based model and we consider 40 taps of transmission line time domain response. For Monte Carlo simulation(MC), we test 10000 sets of random input pattern in order to find the worst-case scenario. On the other hand, our direct solving(DS) algorithm with relaxation-based binary search and linear programming can directly determine the required input pattern for worst-case jitter and noise. Table III shows that, for all the cases, our algorithm obtains more reliable worst-case jitter and noise compared to Monte Carlo simulations. Results show our algorithm obtains worst-case jitter and noise by up to 20% bigger. At the same time, our algorithm is 150× faster.

VI. Conclusion

This paper develops an efficient mathematical method to calculate the worst-case data-dependent jitter and noise directly for a differential microstrip line. We first propose formula-based jitter and noise models that consider the combined effect of ISI, crosstalk and the pre-emphasis filter. With given input patterns, our models achieve within 5% difference compared to SPICE simulation. Furthermore, using these formula-based models, we develop mathematical programming algorithms to directly predict the input patterns that cause worst-case jitter and worst-case amplitude noise. Experiments show our algorithms obtain more reliable worst-case jitter and noise compared to Monte Carlo simulation and, meanwhile, achieve a 150× runtime reduction. Note that our modeling and mathematical programming algorithm are not restricted to differential signaling and can be applied to any multiconductor transmission lines. Moreover, our formula-based models are efficient and are suitable for transmission line automatic synthesis.

TABLE III

WORST-CASE JITTER, AMPLITUDE NOISE AND RUNTIME COMPARISON: MONTE CARLO(MC) AND DIRECT SOLVING(DS).

	Jitter (ps)		Noise (volts)		Runtime (sec)	
	MC	DS	MC	DS	MC	DS
#1	16	16	0.34	0.36	37.8	0.25
#2	8	8	0.25	0.27	38.9	0.25
#3	9	9	0.25	0.30	38.2	0.26
#4	20	24	0.37	0.41	37.8	0.26
#5	12	12	0.14	0.17	37.9	0.26

References

[1] V. Stojanovic and M. Horowitz, "Modeling and analysis of high-speed links," *Custom Integrated Circuits Conference, 2003. Proceedings of the IEEE 2003*, pp. 589–594, Sept. 2003.

[2] J. Buckwalter and A. Hajimiri, "Crosstalk-induced jitter equalization," *Custom Integrated Circuits Conference, 2005. Proceedings of the IEEE 2005*, pp. 409–412, Sept. 2005.

[3] S. Haykin, *Communication Systems*. John Wiley and Sons, 2000.

[4] G. Breed, "Analyzing signals using the eye diagram," *High Frequency Electronics*, pp. 50–53, Nov. 2005.

[5] A. Kuo, R. Rosales, T. Farahmand, S. Tabatabaei, and A. Ivanov, "Crosstalk bounded uncorrelated jitter (buj) for high-speed interconnects," *Instrumentation and Measurement, IEEE Transactions on*, vol. 54, pp. 1800–1810, Oct. 2005.

[6] M. Li, S. Wang, Y. Tao, and T. Kwasniewski, "Fir filter optimisation as pre-emphasis of high-speed backplane data transmission," *Electronics Letters*, vol. 40, pp. 912–913, July 2004.

[7] Y. Tao, W. Bereza, R. Patel, S. Shumarayev, and T. Kwasniewski, "A signal integrity-based link performance simulation platform," *Custom Integrated Circuits Conference, 2005. Proceedings of the IEEE 2005*, pp. 725–728, Sept. 2005.

[8] J. Kim, J. Lee, E. Song, J. Jo, and J. Kim, "Compensation of undesired channel effects by frequency domain optimization of pre-emphasis filter for over gbps signaling," *Electromagnetic Compatibility, 2006. EMC 2006. 2006 IEEE International Symposium on*, vol. 3, pp. 721–726, Aug. 2006.

[9] M. Hashimoto, J. Siriporn, A. Tsuchiya, H. Zhu, and C.-K. Cheng, "Analytical eye-diagram model for on-chip distortionless transmission lines and its application to design space exploration," *Custom Integrated Circuits Conference, 2007. CICC '07. IEEE*, pp. 869–872, Sept. 2007.

[10] V. Popescu, B. Kirei, M. Topa, and C. Munteanu, "Analysis of lossless differential microstrip line," *Electronics Technology, 30th International Spring Seminar on*, pp. 551–554, May 2007.

[11] J. Buckwalter, B. Analui, and A. Hajimiri, "Data-dependent jitter and crosstalk-induced bounded uncorrelated jitter in copper interconnects," *Microwave Symposium Digest, 2004 IEEE MTT-S International*, vol. 3, pp. 1627–1630 Vol.3, June 2004.

[12] N. Ou, T. Farahmand, A. Kuo, S. Tabatabaei, and A. Ivanov, "Jitter models for the design and test of gbps-speed serial interconnects," *Design & Test of Computers, IEEE*, vol. 21, pp. 302–313, July-Aug. 2004.

[13] H. Ymeri, B. Nauwelaers, K. Maex, and D. D. Roest, *"Broadband impedance parameters of symmetric coupled coplanar CMOS interconnects"*. Electrotechnical Review, 2003.

[14] C. R. Paul, *Introduction to electromagnetic compatibility - second edition*. Wiley Interscience, 2006.

[15] R. Achar and M. Nakhla, "Simulation of high-speed interconnects," *Proceedings of the IEEE*, vol. 89, pp. 693–728, May 2001.

[16] K. K. Kim, J. Huang, Y.-B. Kim, and F. Lombardi, "On the modeling and analysis of jitter in ate using matlab," *Defect and Fault Tolerance in VLSI Systems, 2005. DFT 2005. 20th IEEE International Symposium on*, pp. 285–293, Oct. 2005.

[17] W. Beyene and J. Schutt-Aine, "Efficient transient simulation of high-speed interconnects characterized by sampled data," *Components, Packaging, and Manufacturing Technology, Part B: Advanced Packaging, IEEE Transactions on*, vol. 21, pp. 105–114, Feb 1998.

[18] P. Hanumolu, G.-Y. Wei, and U.-K. Moon, "Equalizers for high-speed serial links," *International Journal of High Speed Electronics and Systems*, vol. 15, no. 2, pp. 429–458, 2005.